Neuron
Article

Reduced Synaptic STIM2 Expression and Impaired Store-Operated Calcium Entry Cause Destabilization of Mature Spines in Mutant Presenilin Mice

Suya Sun,[1] Hua Zhang,[1] Jie Liu,[1] Elena Popugaeva,[2] Nan-Jie Xu,[3] Stefan Feske,[4] Charles L. White III,[5] and Ilya Bezprozvanny[1,2,*]
[1]Department of Physiology, UT Southwestern Medical Center at Dallas, Dallas, TX 75390, USA
[2]Laboratory of Molecular Neurodegeneration, Saint Petersburg State Polytechnical University, Saint Petersburg, 195251, Russia
[3]Department of Biochemistry and Molecular Cell Biology, Shanghai Key Laboratory for Tumor Microenvironment and Inflammation, Shanghai Jiao Tong University School of Medicine, Shanghai 200025, China
[4]Department of Pathology, New York University Langone Medical Center, New York, NY 10016, USA
[5]Department of Pathology, UT Southwestern Medical Center at Dallas, Dallas, TX 75390, USA
*Correspondence: Ilya.Bezprozvanny@UTSouthwestern.edu
http://dx.doi.org/10.1016/j.neuron.2014.02.019

SUMMARY

Mushroom dendritic spine structures are essential for memory storage, and the loss of mushroom spines may explain memory defects in Alzheimer's disease (AD). Here we show a significant reduction in the fraction of mushroom spines in hippocampal neurons from the presenilin-1 M146V knockin (KI) mouse model of familial AD (FAD). The stabilization of mushroom spines depends on STIM2-mediated neuronal store-operated calcium influx (nSOC) and continuous activity of Ca^{2+}/calmodulin-dependent protein kinase II (CaMKII). We demonstrate that STIM2-nSOC-CaMKII pathway is compromised in KI neurons, in aging neurons, and in sporadic AD brains due to downregulation of STIM2 protein. We further establish that overexpression of STIM2 rescues synaptic nSOC, CaMKII activity, and mushroom spine loss in KI neurons. Our results identify STIM2-nSOC-CaMKII synaptic maintenance pathway as a novel potential therapeutic target for treatment of AD and age-related memory decline.

INTRODUCTION

The small structures of postsynaptic dendritic spines play an important role in learning and memory (Bourne and Harris, 2008; Kasai et al., 2003). In experimental studies, postsynaptic spines are usually classified into three groups according to their morphological structure: mushroom spines, thin spines, and stubby spines (Bourne and Harris, 2008; Kasai et al., 2003). It has been proposed that the mushroom spines are stable "memory spines" that store memories and that thin spines are "learning spines" that serve as physical substrates for the formation of new memories (Bourne and Harris, 2007). Reflecting the critical role of spines in the formation and storage of memories, significant alterations in spine number and morphology have been observed in a number of neurological and psychiatric disorders (Penzes et al., 2011) and during normal aging (Dickstein et al., 2013).

Most cases of Alzheimer's disease (AD), with memory loss as a cardinal feature, are sporadic and occur in the aging population but in approximately 1%–2% of cases, early onset (<65 years old) AD segregates as an autosomal dominant trait in families (familial AD [FAD]). FAD results from mutations in genes encoding presenilins (PS) or in the amyloid precursor protein (APP). Synapses are lost during AD, correlating strongly with cognitive decline (DeKosky and Scheff, 1990). These studies led to realization that AD is primarily a disease of "synaptic failure" (Knobloch and Mansuy, 2008; Koffie et al., 2011; Luebke et al., 2010; Penzes et al., 2011; Selkoe, 2002; Tackenberg et al., 2009; Wilcox et al., 2011). However, the exact cause of "synaptic failure" in AD remains unknown. Most of the current research in the field has been centered on the idea that elevated levels of amyloid beta Aβ42 peptide lead to elimination of synaptic spines by destabilizing postsynaptic Ca^{2+} signaling or disrupting the network of spine cytoskeleton (Knobloch and Mansuy, 2008; Koffie et al., 2011; Luebke et al., 2010; Penzes et al., 2011; Tackenberg et al., 2009; Wilcox et al., 2011). Since loss of memories is a hallmark of AD, we and others previously proposed that mushroom spines are more likely to be eliminated during AD progression (Bezprozvanny and Hiesinger, 2013; Luebke et al., 2010; Popugaeva and Bezprozvanny, 2013; Popugaeva et al., 2012; Tackenberg et al., 2009). Consistent with these predictions, it has been previously demonstrated that Aβ42 peptide can shift the balance from mushroom to stubby spines in the organotypic hippocampal slice culture preparation (Tackenberg and Brandt, 2009).

Recent amyloid imaging studies indicated that significant fraction of patients display biomarkers of neurodegeneration in the absence of amyloid accumulation in the brain (Jack et al., 2013; Wirth et al., 2013b). In many amyloid-positive patients, there was a poor correlation between local amyloid burden and other neurodegenerative markers (Wirth et al., 2013a). These studies suggested existence of both "amyloid-first" and "neurodegeneration-first" biomarker profile pathways to preclinical AD (Jack et al., 2013; Wirth et al., 2013a, 2013b). If not amyloid, what

can be a driver of pathology in these patients? Our main hypothesis is that neuronal Ca^{2+} dysregulation may play a role of such a driver (Bezprozvanny and Mattson, 2008). The linkage with abnormal Ca^{2+} signaling is particularly strong with FAD mutations in presenilins. Many of PS FAD mutations result in enhanced Ca^{2+} release from endoplasmic reticulum (ER) via inositol 1,4,5-trisphosphate receptors ($InsP_3R$) and ryanodine receptors (RyanR) (Bezprozvanny and Mattson, 2008; Popugaeva and Bezprozvanny, 2013). To explain these findings, we previously proposed that in addition to acting as the catalytic component of the γ-secretase complex, presenilins also function as passive ER Ca^{2+} leak channels, a function that appears to be disrupted by many FAD mutations (Tu et al., 2006). This hypothesis was supported by experimental results from our laboratory (Nelson et al., 2007, 2010; Tu et al., 2006; Zhang et al., 2010), by more recent independent experimental findings (Bandara et al., 2013; Das et al., 2012), and by structural analysis of a bacterial presenilin homolog PSH1 (Li et al., 2013).

We previously predicted (Bezprozvanny and Hiesinger, 2013; Popugaeva and Bezprozvanny, 2013; Popugaeva et al., 2012) that abnormal neuronal Ca^{2+} signaling can cause destabilization of mushroom spines independently form synaptotoxic effects of Aβ42. To test this hypothesis, we focused our studies on PS1-M146V knockin (KI) mice (Guo et al., 1999). This mouse model demonstrates defects in hippocampal memory tasks (Sun et al., 2005; Wang et al., 2004), enhanced early long-term potentiation (E-LTP), and impaired late long-term potentiation (L-LTP) (Auffret et al., 2010). In several studies, abnormal neuronal Ca^{2+} signaling and synaptic transmission abnormalities have been reported for this model (Chakroborty et al., 2009; Goussakov et al., 2010; Stutzmann et al., 2004, 2007; Zhang et al., 2010). Importantly, neuronal Ca^{2+} signaling, synaptic plasticity, and memory defects in these mice occur in the absence of human Aβ42 accumulation, providing an opportunity to study Ca^{2+}-dependent synaptic changes in isolation from synaptotoxic effects of Aβ42.

In the present study, we focused on the analysis of alterations in the shape of synaptic spines in KI hippocampal neurons. The results obtained in our experiments uncovered an essential role of neuronal store-operated Ca^{2+} entry (nSOC) pathway in maintenance of mushroom spines in hippocampal neurons. Our results indicate that nSOC pathway in postsynaptic spines is specifically gated by a stromal interaction molecule 2 (STIM2), an ER Ca^{2+}-sensor protein. We found that nSOC pathway causes persistent activation of Ca^{2+}/calmodulin-dependent protein kinase II (CaMKII) in the spines, and this is needed for long-term stability of mushroom spines. We discovered that this pathway is downregulated in hippocampal neurons from KI mice, in aging mouse neurons, and in human sporadic AD cortical samples. Our results point to STIM2-nSOC-CaMKII synaptic maintenance pathway as a therapeutic target for prevention of synaptic loss in aging brains and in AD.

RESULTS

Reduced Fraction of Mushroom Spines in PS1-M146V KI Hippocampal Neurons

To search for possible structural correlates of memory defects in KI mice, the wild-type (WT) and KI hippocampal cultures were transfected with TD-Tomato plasmid, fixed, and stained with anti-PSD95 antibodies (Figure 1A). PSD95 was localized to the heads of mushroom and stubby spines in both WT and KI neurons, confirming shape-based spine identification (Figure 1A). We observed significant reduction in the fraction of the mushroom spines and proportional increase in the fraction of thin spines in the KI cultures when compared to WT cultures (Figure 1B).

To confirm these findings in vivo, we prepared thick brain slices from WT and KI mice at 3, 6, and 12 months of age and injected lucifer yellow dye (Dumitriu et al., 2011) into hippocampal CA1 neurons to visualize shape of the spines in the secondary apical dendrites of injected cells (Figures S1A available online; Figures 1C, 1E, and 1G). We discovered that the total spine density was significantly higher in 3-month- and 6-month-old KI neurons than in age-matched WT neurons (Figures 1D and 1F). The fraction of mushroom spines was in the range 25%–30% for both WT and KI hippocampal slices at 3 months of age (Figure 1D). By 6 months of age, the fraction of mushroom spines in WT neurons was increased to 40%, significantly higher than in KI neurons at the same age (Figure 1F). The fraction of mushroom spines in 12-month-old WT neurons was reduced to 30%, but was still significantly higher than in KI neurons at the same age (Figure 1H). We did not observe any significant difference in the fraction of stubby spines between WT and KI mice at any age (Figures 1D, 1F, and 1H). The fraction of thin spines was inversely correlated with the fraction of mushroom spines. At 6 and 12 months of age there was a significant increase in the fraction of thin spines in KI neurons when compared to WT neurons (Figures 1F and 1H). Most likely, proliferation of thin spines is responsible for increase in total spine density in KI neurons at this age (Figures 1F and 1H). From this analysis (Figure 1), we concluded that in WT and KI neurons there is an age-dependent shift of a balance away from mushroom spines and toward thin spines.

Postsynaptic nSOC Is Impaired in PS1-M146V KI Hippocampal Neurons

The KI mice do not express human APP protein and do not make human Aβ42. Murine Aβ does not exert synaptotoxic effects. PS1-M146V mutation has only subtle effect on Notch processing (Sun et al., 2005), as has been confirmed in our control experiments with KI hippocampal cultures (data not shown). Thus, neither Aβ42 toxicity nor dysfunction of Notch pathway are likely to cause mushroom spine loss in KI neurons. Abnormal neuronal Ca^{2+} signaling is well documented in KI mice (Chakroborty et al., 2009; Goussakov et al., 2010; Stutzmann et al., 2004, 2007; Zhang et al., 2010). Thus, we turned our attention to potential connection between neuronal Ca^{2+} signaling and stability of mushroom spines. Formation of excitatory spines was increased in transgenic mice that overexpressed TRPC6 channel, a potential component of nSOC entry pathway (Zhou et al., 2008). Impaired function of SOC in presenilin mutant cells was suggested by the previous studies (Akbari et al., 2004; Bojarski et al., 2009; Herms et al., 2003; Leissring et al., 2000; Yoo et al., 2000; Zhang et al., 2010). Thus, we decided to explore a potential role of nSOC.

To quantify nSOC in hippocampal neurons, the amplitude of nSOC-mediated Ca^{2+} influx in the soma was measured by

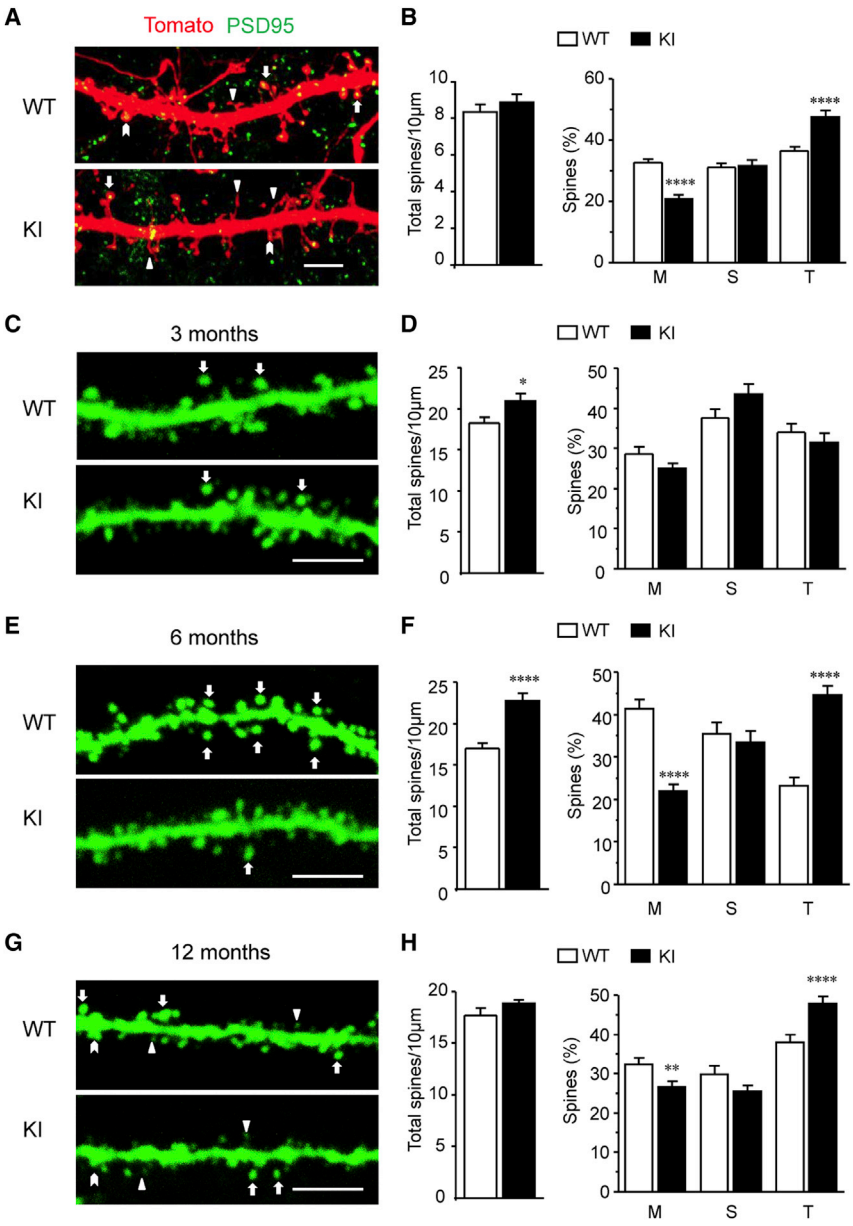

Figure 1. Loss of Mushroom Spines in PS1-M146V KI Hippocampal Neurons

(A) The spine shape of primary hippocampal neurons from WT or KI mice was visualized with TD-Tomato. Subcellular localization of PSD95 was analyzed by immunostaining of hippocampal cultures.

(B) Total spine density and percentage of various spine types in hippocampal neuronal cultures from WT and KI mice. For spine quantification, n = 21–23 neurons (from four batches of cultures) were analyzed for each group.

(C, E, and G) Spine morphology in CA1 hippocampal neurons from 3-month-old (C), 6-month-old (E), and 12-month-old (G) WT and KI mice was visualized by lucifer yellow injections and two-photon imaging.

(D, F, and H) Total spine density and percentage of mushroom (M), stubby (S), and thin (T) spine types in hippocampal neurons from 3-month-old (D), 6-month-old (F), and 12-month-old (H) WT and KI mice. On (A), (C), (E), and (G), mushroom spines are marked by arrows; thin spines are marked by triangles; stubby spines are marked by chevron. Scale bars represent 10 μm in (A) and 5 μm in (C), (E), and (G). n = 3 mice for each group. Values are shown as mean ±SEM. *p < 0.05; **p < 0.01; ****p < 0.0001 by t test.

Fura-2 fluorescence (Figure 2A). Consistent with our previous results obtained with the 3×Tg AD mouse model ($PS1_{M146V}$ KI, Thy1-$APP_{KM670/671NL}$, Thy1-tau_{P301L}) (Zhang et al., 2010), we found that amplitude of somatic nSOC after 2 min depletion protocol was significantly reduced in KI neurons when compared to WT neurons (Figures 2B and 2F). As we discussed previously (Zhang et al., 2010), this result can be explained by impaired ER Ca^{2+} leak function in KI neurons, so that ER Ca^{2+} stores in KI neurons cannot be fully depleted during 2 min incubation in Ca^{2+}-free media, resulting in incomplete activation of nSOC pathway. Measurements of ionomycin-sensitive ER Ca^{2+} pool in KI neurons following 2 min depletion protocol are consistent with this explanation (Figure S2A). To evaluate the function of nSOC pathway independently from the differences in the filling state of the Ca^{2+} stores, we extended the length of incubation in Ca^{2+}-free media to 30 min to allow complete ER Ca^{2+} store depletion in both cultures. We discovered that following 30 min depletion protocol the amplitude of somatic nSOC was similar in WT and KI cultures (Figures 2C and 2F). Thus, we concluded that the function of somatic nSOC pathway is minimally affected in KI neurons in conditions of complete ER Ca^{2+} store depletion.

It is well established that Ca^{2+} signaling in dendritic spines is compartmentalized and relatively insulated from somatic Ca^{2+} signaling (Higley and Sabatini, 2012; Kasai et al., 2003; Yasuda et al., 2003). Thus, we decided to study function of nSOC pathway in the spines. To perform Ca^{2+} imaging in the spines, we transfected hippocampal neurons with GCamp5.3 plasmid that encodes genetically encoded Ca^{2+} indicator (Tian et al., 2009), which enabled us to simultaneously visualize the dendritic spines and to measure local Ca^{2+} signals (Figure 2D; Movie S1). Following 30 min incubation in Ca^{2+}-free media, we discovered that nSOC signals were greatly attenuated in the spines from KI neurons when compared to WT spines (Figures 2E and 2F). These results suggested that some components of nSOC pathway were significantly impaired in the spines, but not in the soma, of KI hippocampal neurons. To further confirm these findings, we compared amplitude of synaptic nSOC in spines from 2-months-old WT and KI hippocampal slices. In these experiments WT and KI mice were stereotaxically injected with adeno-associated virus (AAV) encoding GCamp5.3, and the

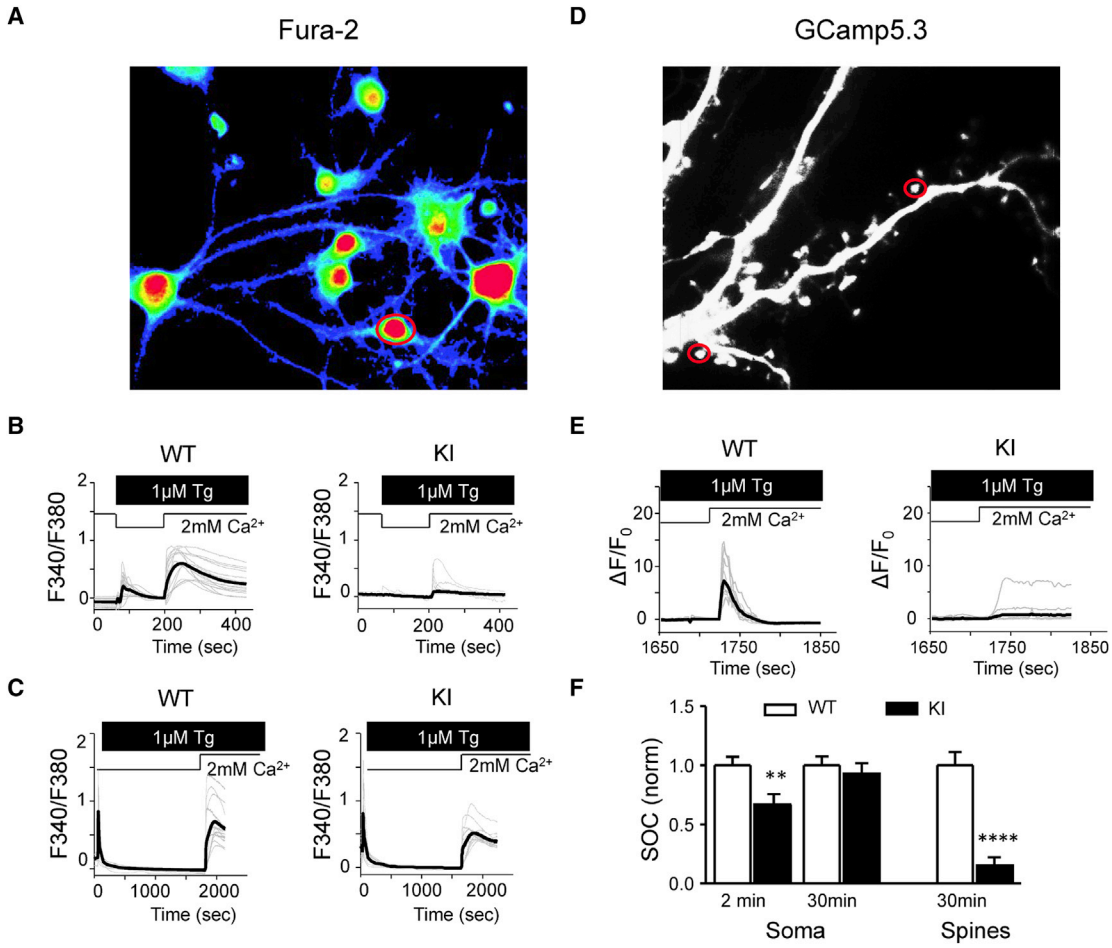

Figure 2. Reduced Synaptic Store-Operated Ca^{2+} Entry in PS1-M146V KI Hippocampal Neurons

(A) Fura-2 fluorescence in live hippocampal neurons. Somatic ROI is shown by a red circle.

(B and C) Time course of Fura-2 Ca^{2+} signals (F340/F380) is shown for WT and KI hippocampal neurons following 2 min (B) or 30 min (C) store-depletion protocol.

(D) GCaMP5.3 fluorescence in live hippocampal neurons. The samples for synaptic ROI are shown by a red circle.

(E) Time course of synaptic GCaMP5.3 Ca^{2+} signals ($\Delta F/F_0$) is shown for WT and KI hippocampal neurons following 30 min store-depletion protocol. In (B), (C), and (E), individual cell traces (gray) and average traces (black) are shown for each experimental group.

(F) The average peak SOC responses in soma and spines of WT and KI hippocampal neurons (normalized to WT). Values are shown as mean ±SEM. (All the data was collected from three to five batches of cultures.) $^{**}p < 0.01$; $^{****}p < 0.0001$ by t test.

spine nSOC amplitude was measured in live slices by two-photon Ca^{2+} imaging. Obtained results confirmed that synaptic SOC is impaired in spines of KI neurons when compared to WT neurons (Figures S2C and S2D).

Spine shape analysis and Ca^{2+} imaging experiments suggested that PS1-M146V KI mutation results in destabilization of mushroom spines (Figure 1) and impaired synaptic nSOC (Figure 2). We further extended our analysis to four additional PS1-FAD mutants: L166P, A246E, E273A, and A426P. In the previous studies we demonstrated that all of these four mutations disrupt ER Ca^{2+} leak function of PS1 (Nelson et al., 2010). As KI mouse models for these mutants are not available, we expressed these mutants in WT hippocampal neuronal cultures and discovered that the fraction of mushroom spines was significantly reduced, and postsynaptic nSOC was suppressed in neurons expressing any of these PS1-FAD mutants (Figures S1B, S1C, and S2B). From these results we concluded that impaired ER Ca^{2+} leak function due to PS1-FAD mutations results in impaired synaptic nSOC and destabilization of mushroom spines in PS1-FAD hippocampal neurons.

STIM2 Protein Is Downregulated in PS1-M146V KI, APPPS1, Aging, and AD Neurons

SOC pathway is activated in response to reduced levels of Ca^{2+} in the ER due to activation of stromal interaction molecules (STIMs), ER-resident Ca^{2+}-sensor proteins. Two mammalian isoforms of STIM proteins (STIM1 and STIM2) differ in their affinity for ER Ca^{2+} and expression pattern (Collins and Meyer, 2011). In order to identify the components of nSOC affected in KI neurons, we performed western blotting analysis of STIMs and transient receptor potential channel 1 (TRPC1), a potential component of nSOC pathway (Riccio et al., 2002; Wu et al., 2011), in lysates

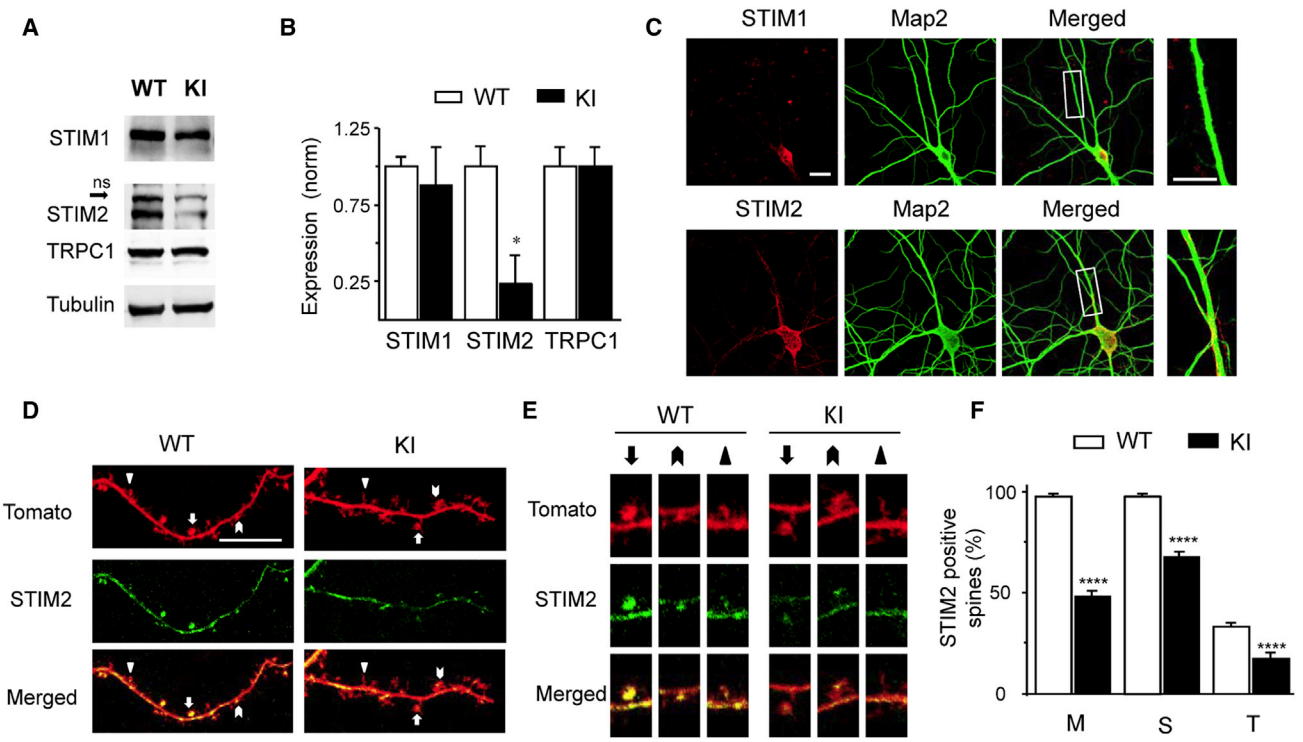

Figure 3. Downregulation of STIM2 Protein in PS1-M146V KI Hippocampal Neurons

(A) The expression levels of STIM1, STIM2, and TRPC1 protein were analyzed by western blotting of lysates from WT and KI hippocampal cultures. Tubulin was used as loading control. ns indicates nonspecific band.

(B) Quantification of STIM1, STIM2 and TRPC1 expression levels in WT and KI cultures (normalized to tubulin levels).

(C) Subcellular localization of STIM1 and STIM2 were analyzed by immunostaining of hippocampal cultures. MAP2 was used for neuronal labeling. Scale bar indicates 10 μm.

(D and E) STIM2 localization in WT and KI neurons transfected with TD-Tomato. Mushroom spines are marked by arrows; thin spines are marked by triangles; stubby spines are marked by chevron. The scale bars in (D) represent 20 μm in the left panels and 10μm in the right panel.

(F) The fraction of STIM2-positive spines is shown for mushroom (M), stubby (S), and thin (T) spines in WT and KI neurons. All the data was collected from three batches of cultures. Values are shown as mean ±SEM. *$p < 0.05$; ****$p < 0.0001$ by t test.

prepared from WT and KI hippocampal cultures. In these experiments, we discovered that the expression levels of STIM2, but not of STIM1, were dramatically reduced in KI hippocampal cultures when compared to WT cultures (Figures 3A and 3B). The levels of TRPC1 protein were similar in WT and KI cultures (Figures 3A and 3B). It has been reported that both STIM1 and STIM2 proteins are expressed in the nervous system (Gruszczynska-Biegala et al., 2011; Skibinska-Kijek et al., 2009), with STIM2 highly enriched in hippocampal neurons (Figure S3). To further understand unique roles of STIM1 and STIM2 in hippocampal neurons, we performed a series of immunostaining experiments with primary hippocampal neuronal cultures. In these experiments, we discovered that STIM1 protein is restricted to the neuronal soma, whereas STIM2 is broadly expressed and present in both soma and dendrites (Figure 3C). To evaluate localization of STIM2 in the spines, we transfected WT and KI cultures with TD-Tomato construct and stained the cultures with antibodies against STIM2 protein (Figure 3D). We used confocal images of TD-Tomato to identify various types of spines (Figure 3E) and scored every spine as "STIM2-positive" or "STIM2-negative." From this analysis we established that STIM2 protein was present in almost all mushroom and stubby spines, but not in thin spines, in WT cultures (Figures 3E and 3F). In agreement with the western blotting data (Figures 3A and 3B), we found that the levels of STIM2 protein were significantly reduced in spines of KI hippocampal neurons (Figures 3E and 3F).

To further test generality of these findings, we performed western blotting analysis of hippocampal lysates from 3-, 6-, and 12-month-old WT and KI mice (Figures 4A, 4B, S4A, and S4B). Consistent with hippocampal culture data (Figures 3A and 3B), we found that the levels of STIM1 and TRPC1 proteins were similar in 3-, 6-, and 12-month-old WT and KI hippocampal samples, but the levels of STIM2 protein were significantly reduced in 6- and 12-month-old KI hippocampal samples (Figures 4A, 4B, and S4B). To further validate these findings, we evaluated expression of STIM proteins in hippocampal lysates from APPPS1 mice ($APP_{KM670/671NL}$, $PS1_{L166P}$) (Radde et al., 2006), a different model of AD. Similar to results with KI mice, we observed specific downregulation of STIM2 protein in hippocampal lysates from 9-month-old APPPS1 mice (Figures S4C and S4D). While performing analysis with FAD mouse models, we noticed that even for WT mice, levels of STIM2 protein

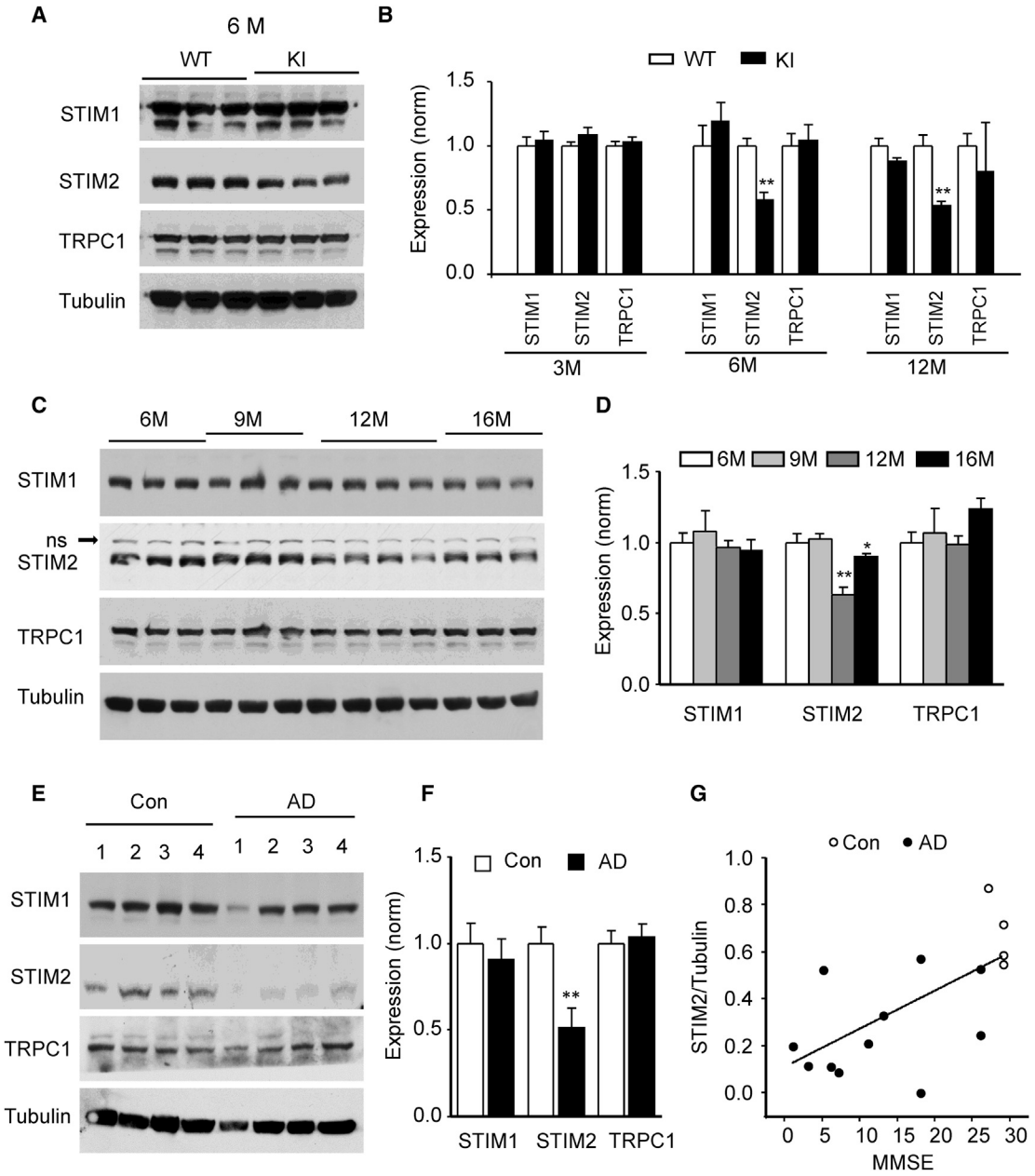

Figure 4. Downregulation of STIM2 Protein in PS1-M146V KI and Aging Mice Hippocampus and in Cortex of Alzheimer's Patients

(A) The expression levels of STIM1, STIM2 and TRPC1 proteins were analyzed by western blotting of hippocampal lysates from 6-month-old WT and KI mice.

(B) Quantification for western blotting data shown in (A) and Figures S4A and S4B.

(C) The expression levels of STIM1, STIM2, and TRPC1 proteins were analyzed by western blotting of hippocampal lysates from 6-, 9-, 12-, and 16-month-old WT mice.

(D) Quantification of western blotting data shown in (C).

(E) The expression levels of STIM1, STIM2, and TRPC1 proteins were analyzed by western blotting of normal human (Con) and AD patient's (AD) cortical lysates.

(F) Quantification of western blotting data shown in (E) and Figure S4E.

(G) Correlation between STIM2 levels and MMSE scores. The STIM2 expression levels (normalized to tubulin) were plotted versus MMSE score for each AD patient (filled circles) and four control subjects (open circles). Straight line is a linear fit to all 15 data points ($r^2 = 0.38$). Tubulin was used as a loading control in all western blots, and signal intensity of STIM1, STIM2, and TRPC1 bands was normalized to tubulin level in the same sample. Sample in each column was from individual mouse or human tissue. Average values are shown as mean ±SEM (n = 3 mice and 11 human tissues for each group). *$p < 0.05$; **$p < 0.01$ by t test or one-way ANOVA followed by Tukey's test.

were reduced in 12-month-old samples when compared to 3- and 6-month-old samples. To confirm and extend these findings, we performed systematic western blotting analysis of hippocampal samples from another group of WT mice at 6, 9, 12, and 16 months of age. We found that the levels of STIM1 and TRPC1 proteins remained unchanged as a function of age (Figures 4C and 4D). In contrast, levels of STIM2 protein were significantly reduced in 12- and 16-month-old hippocampal samples (Figures 4C and 4D). These experiments lead us to conclude that STIM2 levels are reduced in hippocampus of aging and FAD mice.

To establish relevance of our findings for human disease, we obtained human cortical samples from a group of 11 sporadic AD patients and 11 age-matched controls (clinical and pathological information about these samples is summarized in Table S1). We performed a series of western blotting experiments with the human cortical lysates (Figures 4E and S4E). From analysis of obtained results, we concluded that STIM2 expression levels were significantly reduced in AD samples when compared to age-matched controls (Figure 4F). In contrast, levels of TRPC1 and STIM1 proteins were not significantly affected in AD samples (Figure 4F). To establish a potential correlation between STIM2 expression levels and disease progression, we plotted STIM2 expression levels (normalized to tubulin) versus MMSE score for each AD patient and four control subjects for which MMSE scores were available (Table S1). We observed significant correlation (r^2 = 0.38) between STIM2 levels and MMSE scores (Figure 4G), indicating that reduced STIM2 levels correlate with severity of the disease. We also performed analysis of STIM2 expression levels in the cortical samples from six MCI patients, but we did not observe significant reduction in STIM2 levels (data not shown), most likely because these patients were at the very early stages of the disease, as evidenced by their MMSE scores (Table S1). From obtained results, we concluded that STIM2 downregulation occurs in neurons from PS1-M146V KI mice, in neurons from APPPS1 mice, in aging neurons, and in sporadic AD neurons.

STIM2-nSOC Pathway Is Necessary for Mushroom Spine Stability

To directly evaluate the role of STIM2-nSOC pathway in stabilization of mushroom spines, we took a genetic approach. For these experiments we used conditional knockout (cKO) mice of the *Stim2* gene (Oh-Hora et al., 2008). Hippocampal neurons from *Stim2*$^{fl/fl}$ mice were infected with lentiviruses encoding nuclear-targeted Cre (NLS-Cre) to generate *Stim2* cKO neurons. Western blotting of lysates obtained from the infected cultures confirmed efficient and specific knockout of STIM2 protein in NLS-Cre-infected *Stim2*$^{fl/fl}$ hippocampal neurons, with minimal effect on STIM1 expression levels (Figure 5C). To determine functional effects of STIM2 deletion, we evaluated nSOC activity in soma and spines of Cre-transduced *Stim2*$^{fl/fl}$ neurons. We found that deletion of STIM2 resulted in 35% reduction in the average amplitude of somatic nSOC (Figures 5A and 5B). The amplitude of synaptic nSOC was dramatically reduced in the absence of STIM2 (Figures 5A and 5B), with the average amplitude of synaptic nSOC reduced by 85% in *Stim2* cKO neurons (Figures 5A and 5B). These results indicated that STIM2 is predominantly responsible for synaptic nSOC, in agreement with subcellular localization analysis (Figure 3).

To study the effect of STIM2 deletion and synaptic nSOC reduction on mushroom spine stability, GFP- or Cre-transduced *Stim2*$^{fl/fl}$ neurons were transfected with TD-Tomato, and the shape of spines was analyzed by confocal imaging (Figure 5D). We found that the overall spine density was similar in GFP- and Cre-transduced cultures (Figure 5E), just as we had observed for WT and KI cultures (Figure 1B). Also similar to KI cultures, the fraction of mushroom spines was significantly reduced, and the fraction of thin spines was proportionally increased in *Stim2* cKO neurons (Figure 5E). These results are consistent with our hypothesis that STIM2-mediated synaptic nSOC pathway plays an important role in the stabilization of mushroom spines.

To validate these findings in vivo, we performed stereotaxic injections of AAV1-NLS-Cre viruses and control AAV1-NLS-GFP viruses to the hippocampal region of 2-month-old *Stim2*$^{fl/fl}$ mice. Efficient and specific knockout of STIM2 protein in these experiments was confirmed by western blotting of hippocampal lysates prepared 4 weeks after viral injections (Figure 5F). For analysis of spine morphology GFP- and Cre-injected mice were sacrificed at 4 months of age, and spine morphology was evaluated by lucifer yellow injection procedure combined with two-photon imaging (Figure 5G). Similar to 6-month-old KI mice, we found that the fraction of mushroom spines in *Stim2* cKO mice was significantly reduced, and the fraction of thin spines was proportionally increased (Figure 5H). Thus, in agreement with our hypothesis, knockout of STIM2 and reduction in synaptic nSOC leads to reduction in the fraction of mushroom spines in both culture and slice experiments. When analysis was extended to 6-month-old mice, we observed massive neuronal loss in *Stim2* cKO mice hippocampus (Figure S5), suggesting that STIM2-mediated nSOC pathway is necessary for long-term neuronal survival.

STIM2 Overexpression Rescues Mushroom Spine Deficiency in PS1-M146 KI Hippocampal Neurons

If downregulation of STIM2 is responsible for reduction in synaptic nSOC and loss of mushroom spines, then overexpression of STIM2 should be able to rescue synaptic nSOC and increase mushroom spines in KI neurons. To test these predictions, we coexpressed mouse STIM1 (mSTIM1) and STIM2 (mSTIM2) proteins and control NLS-GFP protein with GCamp5.3 plasmid in hippocampal cultures from WT and KI mice. Consistent with the previous results (Figures 2E and 2F), synaptic nSOC was significantly smaller in GFP-transfected KI cultures than in GFP-transfected WT cultures (Figures 6A and 6B). Expression of mSTIM1 resulted in ~50% increase in the amplitude of synaptic nSOC in both WT and KI cultures (Figures 6A and 6B). Transfection with mSTIM2 resulted in 4- to 5-fold increase in the amplitude of synaptic nSOC in WT and KI cultures (Figures 6A and 6B). Thus, consistent with our hypothesis, overexpressed STIM2 was much more effective in modulating synaptic nSOC activity in WT and KI cultures than STIM1. To evaluate the effects of STIMs on neuron morphology, we cotransfected WT and KI hippocampal neurons with TD-Tomato plasmid and mSTIM1 or mSTIM2 expression plasmids or control NLS-GFP plasmid

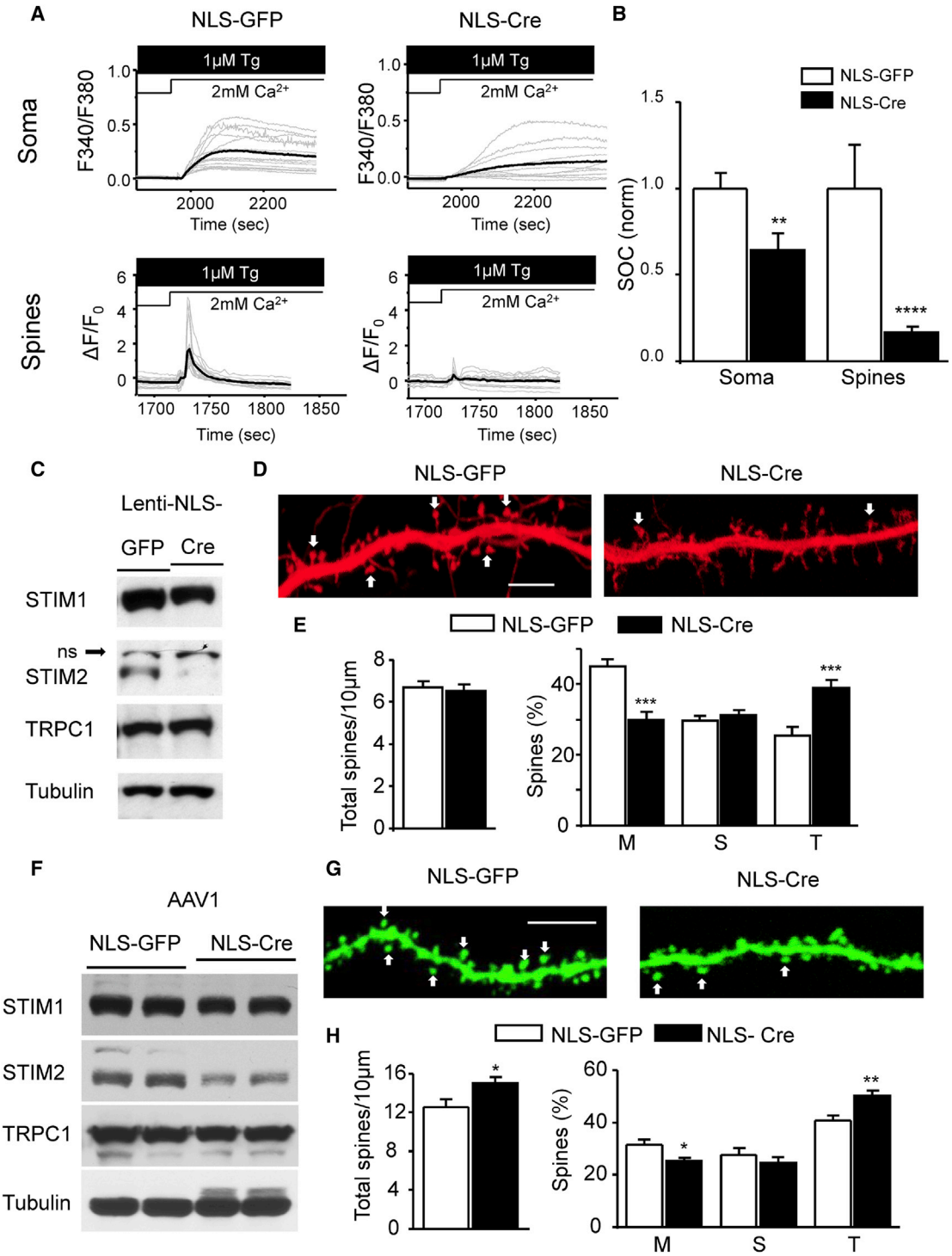

Figure 5. Genetic Deletion of STIM2 Causes Impaired nSOC and Loss of Mushroom Spines in Hippocampal Neurons

(A) Time course of Fura-2 Ca^{2+} signal in the soma and GCamP5.3 Ca^{2+} signal in the spines are shown for *Stim2*$^{fl/fl}$ hippocampal neurons transduced with NLS-GFP or NLS-Cre, as indicated. Individual cell traces (gray) and average trace (black) are shown for each group.

(B) The average peak SOC responses in soma and spines of *Stim2*$^{fl/fl}$ hippocampal neurons transduced with NLS-GFP or NLS-Cre (normalized to NLS-GFP).

(C) Expression levels of STIM1, STIM2, and TRPC1 were analyzed by western blotting of lysates prepared from *Stim2*$^{fl/fl}$ hippocampal cultures infected with Lenti-NLS-GFP or Lenti-NLS-Cre, as indicated. Tubulin was used as a loading control. ns is a nonspecific band.

(D) Spine morphology of the primary hippocampal neurons from *Stim2*$^{fl/fl}$ mice transduced with NLS-GFP or NLS-Cre was visualized with TD-tomato. Mushroom spines are marked by arrows. Scale bar indicates 10 μm.

(legend continued on next page)

(Figure 6C). We discovered that expression of STIM1 had no effect on spine density when compared to expression of GFP (Figures 6C and 6D). Expression of STIM2 resulted in significant decrease in total spine density in both WT and KI cultures (Figures 6C and 6D). When spine shapes were analyzed, we discovered that mSTIM1 overexpression resulted in strong reduction of mushroom spine fraction in WT cultures and in smaller reduction of mushroom spine fraction in KI cultures (Figures 6C and 6D). In contrast, expression of mSTIM2 resulted in small decrease of mushroom spine fraction in WT cultures but an increase in mushroom spine fraction in KI cultures (Figures 6C and 6D).

Synaptic protein PSD95 is enriched in mushroom spines (Figure 1A), and we reasoned that abundance of PSD95 can be used as an alternative readout for mushroom spine density. We found that infection with mSTIM1-encoding lentiviruses had no effect on PSD95 levels in WT cultures and resulted in some elevation of PSD95 levels in KI cultures (Figures 6E and 6F). In contrast, infection with mSTIM2-encoding lentiviruses resulted in significant elevation of PSD95 levels in KI cultures (Figures 6E and 6F). Levels of TRPC1 protein remained unchanged following overexpression of mSTIM1 or mSTIM2 (Figures 6E and 6F). These results supported important and specific role of STIM2 protein in control of postsynaptic spines, in agreement with spine quantification data (Figures 6C and 6D). In parallel control experiments we demonstrated that infection with Lenti-STIM2 viruses had no significant effect on Notch processing in WT and KI hippocampal cultures (data not shown), indicating that the rescue of mushroom spines and PSD95 levels in KI neurons was not due to effects of STIM2 on the γ-secretase activity.

To determine if STIM2 overexpression can rescue mushroom spine deficit in vivo, we performed stereotaxic bilateral injections of AAV1-mSTIM2 viruses or control AAV1-NLS-GFP viruses to hippocampal region of 2-month-old WT or KI mice. Expression of mSTIM2 protein was confirmed by western blotting of hippocampal lysates (Figure 6I). We prepared hippocampal slices from the injected mice at 6 months of age for the analysis of the spine morphology by two-photon imaging (Figure 6G). From this analysis, we determined that mSTIM2 overexpression had no effect on the fraction of mushroom spines in WT mice but rescued the fraction of mushroom spines in KI mice to the WT levels (Figures 6G and 6H). To further validate these findings, we performed a series of western blotting experiments with hippocampal lysates from these mice. Consistent with mushroom spine quantification data, we observed rescue of PSD95 levels in KI mice injected with AAV1-mSTIM2 viruses (Figures 6I and 6J).

CaMKII Acts Downstream of STIM2-nSOC Pathway in the Mushroom Spines

CaMKII is highly concentrated in the postsynaptic density fraction of the spines (Feng et al., 2011). Critical role of CaMKII in LTP-induced formation of mushroom spines has been extensively documented (Lisman et al., 2012; Murakoshi and Yasuda, 2012). In contrast, very limited information exists about potential role of CaMKII in spine stabilization (Sanhueza et al., 2011). Following Ca^{2+}-dependent activation, CaMKII undergo *trans*-autophosphorylation on Thr-286, which enables CaMKII to maintain activity for extended periods of time independently from Ca^{2+} levels. Therefore, abundance of autophosphorylated form can be used as a biochemical indicator of steady-state activity levels of CaMKII. To compare functional state of CaMKII in WT and KI hippocampal cultures, we performed western blotting experiments with CaMKII antibodies and with antibodies specific for phosphorylated form of CaMKII. Consistent with our predictions, we found that the total levels of CaMKII were similar in WT and KI cultures, but the levels of pCaMKII were significantly reduced in KI cultures (Figure 7A). Importantly, the CaMKII autophosphorylation in both WT and KI neurons was abolished by short-term application of SOC inhibitors SKF96365 or 2APB (Figure 7A), suggesting that continuous nSOC activity is needed to maintain CaMKII in the phosphorylated state. Immunostaining results confirmed colocalization of pCaMKII and STIM2 in mushroom spines of hippocampal neurons in culture (Figure S6A). Reduction in pCaMKII in our experiments was closely matched by reduction in PSD95 levels (Figure 7A), suggesting that blockage of nSOC causes loss of mature spines. To further validate results obtained with pharmacological inhibitors of SOC, we utilized a genetic strategy. We discovered that the levels of pCaMKII and PSD95 were reduced in hippocampal cultures from *Stim2*$^{fl/fl}$ mice infected with Lenti-Cre viruses (Figure 7A). Similar results were obtained with hippocampal lysates from *Stim2*$^{fl/fl}$ mice injected with AAV1-Cre viruses (Figure 7A). In addition to the observation that STIM2 levels were reduced in aging hippocampus (Figure 4C), in western blotting experiments with hippocampal lysates from the aging mice we observed significant reduction in pCaMKII and PSD95 levels in 12-month-old samples (Figures 7B and 7C), consistent with impaired nSOC signaling in the spines. Reduced levels of synaptic pCaMKII were reported for hippocampus of human MCI and AD patients (Reese et al., 2011), consistent with our observations. Overexpression of STIM2 resulted in rescue of pCaMKII levels in hippocampal cultures from KI mice (Figures 7D and 7E). Consistent with nSOC rescue experiments (Figures 6A and 6B), expression of STIM2 had more potent effect on pCaMKII levels in KI neurons

(E) Total spine density and percentage of various spine types in hippocampal neuronal cultures from *Stim2*$^{fl/fl}$ mice transduced with NLS-GFP or NLS-Cre. M indicates mushroom, S indicates stubby, and T indicates thin. For spine quantification, n = 18–20 neurons were analyzed. The data were collected from four batches of cultures for each group.

(F) Expression levels of STIM1, STIM2, and TRPC1 were analyzed by western blotting of hippocampal lysates prepared from *Stim2*$^{fl/fl}$ mice injected with AAV1-NLS-GFP or AAV1-NLS-Cre, as indicated. Tubulin was used as a loading control. Each sample was from individual mouse.

(G) Spine morphology in hippocampal neurons from 4-month-old *Stim2*$^{fl/fl}$ mice injected with AAV1-NLS-GFP or AAV1-NLS-Cre was visualized by lucifer yellow injections and two-photon imaging. The infected neurons were identified by GFP fluorescence. Mushroom spines are marked by arrows. Scale bar indicates 5 μm.

(H) Total spine density and percentage of various spine types in hippocampal slices from 4-month-old *Stim2*$^{fl/fl}$ mice injected with AAV1-NLS-GFP or AAV1-NLS-Cre (n = 4 mice for each group). M indicates mushroom, S indicates stubby, and T indicates thin. Values are shown as mean ±SEM. *$p < 0.05$; **$p < 0.01$; ***$p < 0.001$; ****$p < 0.0001$ by t test.

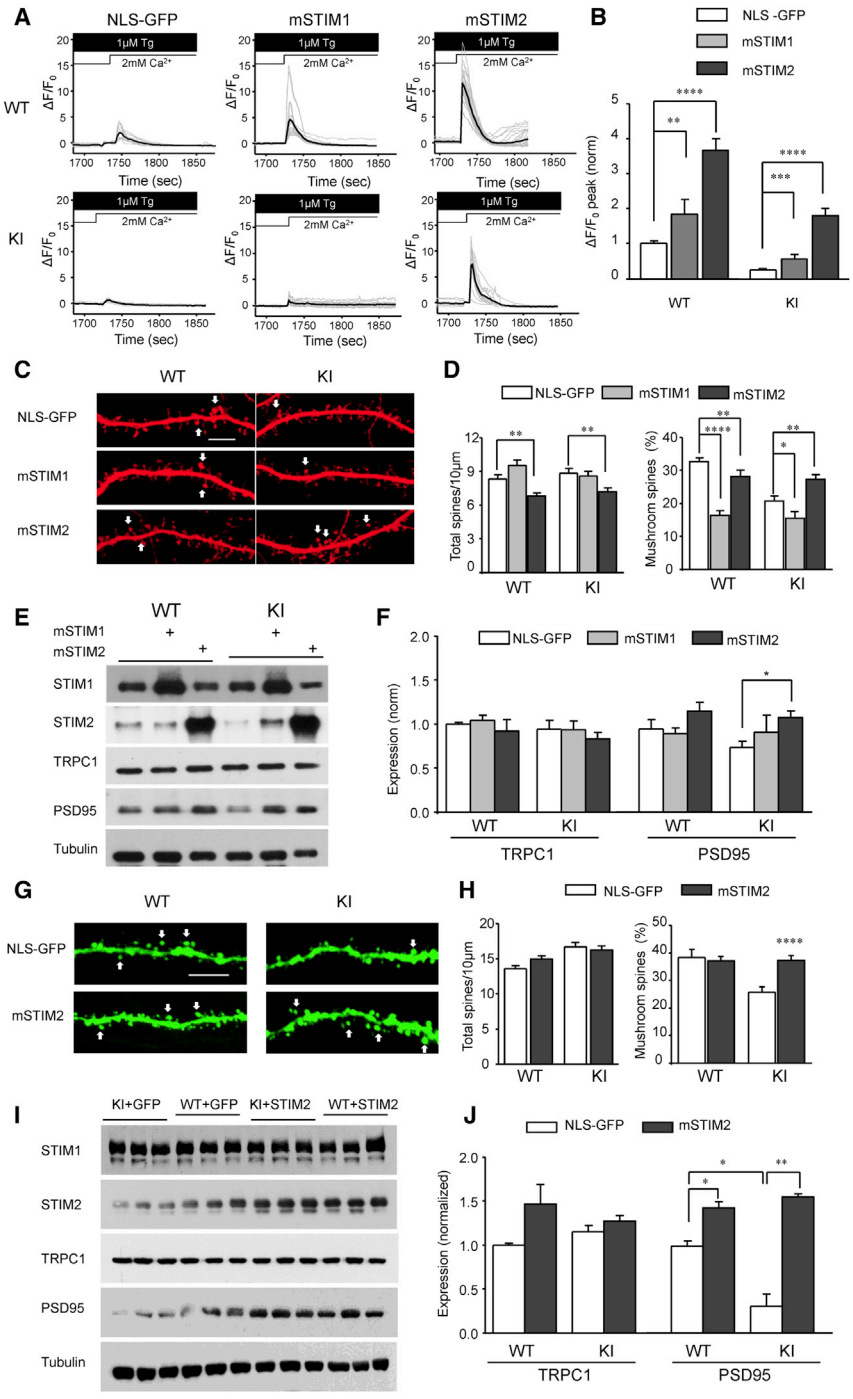

Figure 6. Overexpression of STIM2 Rescues Synaptic nSOC and Mushroom Spine Deficit in Hippocampal Neurons from PS1-M146V KI Mice

(A) Time course of GCamP5.3 Ca^{2+} signal in the spines of WT and KI hippocampal neurons transfected with NLS-GFP, mSTIM1, and mSTIM2, as indicated. Individual cell traces (gray) and average trace (black) are shown for each group.

(B) The peak SOC responses in spines of WT and KI hippocampal neurons transfected with NLS-GFP, mSTIM1, and mSTIM2, as indicated. The values of $\Delta F/F_0$ signals were averages for each group of cells.

(C) The spine morphology of WT and KI primary hippocampal neurons transfected with NLS-GFP, mSTIM1, or mSTIM2 was visualized with TD-tomato. Mushroom spines are marked by arrows. Scale bar indicates 10 μm.

(D) Total spine density and percentage of mushroom spines in WT and KI hippocampal neuronal cultures transfected with NLS-GFP, mSTIM1, or mSTIM2. For spine quantification, n = 15–24 neurons were analyzed. The data were collected from four batches of cultures.

(E) The expression levels of STIM1, STIM2, TRPC1, and PSD95 proteins were analyzed by western blotting of cultured hippocampal neurons which overexpress mSTIMs by lentivirus.

(F) Quantification of TRPC1 and PSD95 proteins for western blotting data.

(G) Spine morphology in hippocampal neurons from 6-month-old WT and KI mice that were injected with AAV1-NLS-GFP or AAV1-mSTIM2 was visualized by lucifer yellow injections and two-photon imaging. Mushroom spines are marked by arrows. Scale bar indicates 5 μm.

(H) Percentage of mushroom spines in hippocampal slices from 6-month-old WT and KI mice injected with AAV1-NLS-GFP or AAV1-mSTIM2 (n = 4 mice for each group).

(I) The expression levels of STIM1, STIM2, TRPC1, and PSD95 proteins were analyzed by western blotting of hippocampal lysates from STIM2 rescued KI mice and control mice.

(J) Quantification of TRPC1 and PSD95 for western blotting data shown in (I). Values are shown as mean ±SEM. *$p < 0.05$; **$p < 0.01$; ***$p < 0.001$; ****$p < 0.0001$ by one-way ANOVA or two-way ANOVA followed by Tukey's test.

than expression of STIM1 (Figures 7D and 7E). Furthermore, we demonstrated that AAV1-mediated expression of STIM2 rescued pCaMKII levels in hippocampus of KI mice in vivo (Figures 7F and 7G). Expression of STIM2 in vivo had no effect on total CaMKII levels in both groups or the levels of pCaMKII in WT hippocampus (Figures 7F and 7G), validating specificity of effects observed in KI brain.

Obtained results suggested that impairment of CaMKII activity in KI neurons occurs downstream from impairment in STIM2-nSOC synaptic Ca^{2+} influx. There are many downstream targets of CaMKII that may play a role in stabilization of mushroom spines (Lisman et al., 2012; Murakoshi and Yasuda, 2012). In our studies, we focused on small GTPase proteins Cdc42 and Rac1, which play an important role in actin cytoskeleton reorganization in the spines. During LTP paradigm, Cdc42/Rac1 are activated in spines downstream of CaMKII (Murakoshi and Yasuda, 2012). To quantify Cdc42/Rac1 activity in KI spines, we prepared lysates from WT and KI cultures and isolated GTP-bound active form of Cdc42 and Rac1 proteins by pull-down with GST-PAK1-PBD beads (Knaus et al., 2007). We found that the

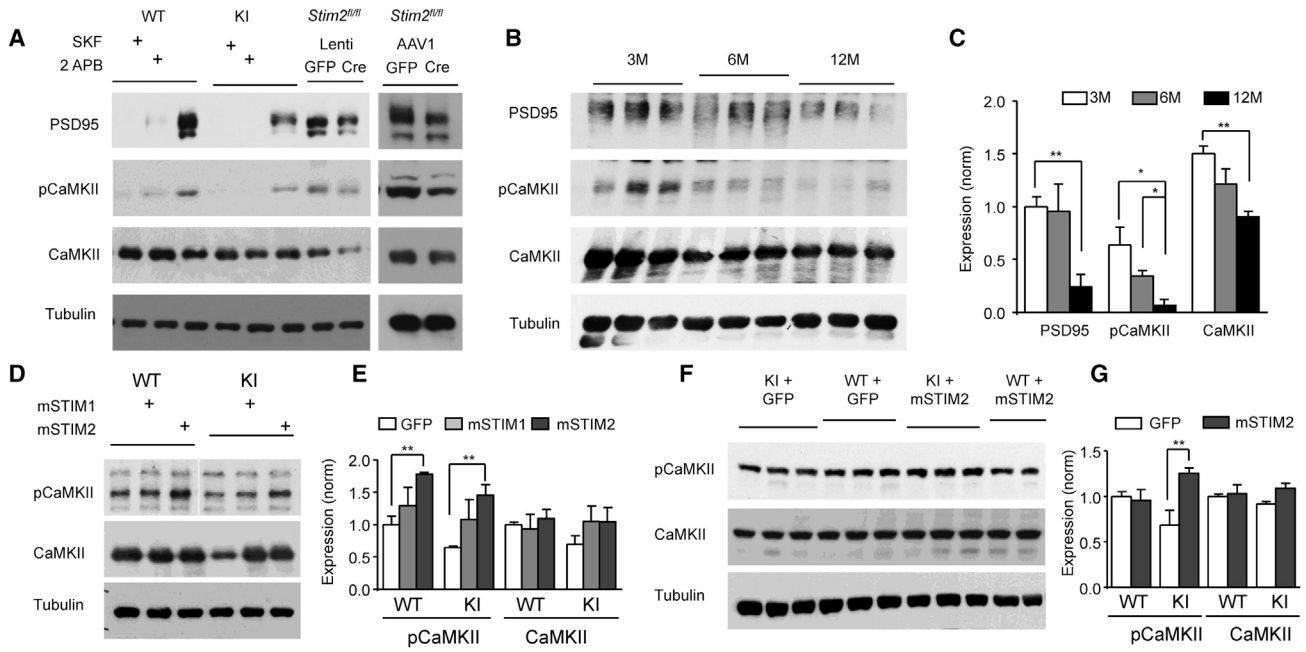

Figure 7. Synaptic CaMKII as Downstream Target for STIM2-nSOC Pathway

(A) Analysis of PSD95, pCaMKII, and CaMKII levels in WT and KI hippocampal neurons treated with nSOC inhibitors (SKF96365, 30 μM and 2-APB, 30 μM) for 16 hr and in *Stim2*$^{fl/fl}$ neurons transduced with NLS-Cre and NLS-GFP in vitro and in vivo.

(B) The levels of PSD95, pCaMKII, and CaMKII were analyzed by western blotting of hippocampal lysates from 6-month-, 9-month-, and 12-month-old WT mice. Sample in each lane was from individual mouse.

(C) Quantification of western blotting data shown in (B).

(D) The expression levels of pCaMKII and CaMKII levels proteins were analyzed by western blotting of cultured hippocampal neurons which overexpress mSTIMs by lentivirus.

(E) Quantification of pCaMKII and CaMKII levels proteins for western blotting data in (D).

(F) The expression levels of pCaMKII and CaMKII proteins were analyzed by western blotting of hippocampal lysates from STIM2 rescued KI mice and control mice.

(G) Quantification of pCaMKII and CaMKII for western blotting data shown in (F).

Tubulin was used as a loading control in all western blotting experiments. Average values are shown as mean ±SEM (n = 3 mice or batches for each group). *p < 0.05; **p < 0.01, by one-way or two-way ANOVA followed by Tukey's test.

levels of activated Cdc42/Rac1 were indeed reduced in lysates from KI neurons when compared to WT neurons (Figure S6B). Importantly, levels of activated Cdc42/Rac1 in KI neurons were rescued by infection of KI cultures with STIM2 lentiviruses but not with STIM1 lentiviruses (Figure S6B). These results supported the hypothesis that impaired function of STIM2-nSOC-CaMKII pathway resulted in reduced levels of active Cdc42/Rac1 in KI hippocampal spines.

DISCUSSION

STIM2-nSOC-CaMKII Pathway and Stability of Mushroom Postsynaptic Spines

It has been proposed that the mushroom spines play an important role in storage of memories (Bourne and Harris, 2007; Kasai et al., 2003). There is an extensive literature related to spine growth and formation of mushroom spines following LTP-inducing stimulation paradigms (Lisman et al., 2012; Murakoshi and Yasuda, 2012). In contrast, relatively little is known about signaling mechanisms involved in long-term maintenance of mushroom spines (Bezprozvanny and Hiesinger, 2013; Sanhueza et al., 2011). Based on the results obtained in the current study, we would like to propose an existence of a novel signaling pathway involved in long-term stabilization of mushroom spines in healthy neurons (Figure 8A). Our results indicate that the maintenance of individual mushroom spines depends on continuous levels of CaMKII activity in these spines (Figure 8A). Although postsynaptic spines contain multiple potential sources of Ca^{2+} influx, such as NMDAR, AMPAR, and VGCC (Murakoshi and Yasuda, 2012), these channels provide rapid and massive Ca^{2+} influx during stimulation and remain silent at rest. Thus, these channels are poorly suited to support long-term maintenance mechanism. Instead, our data indicate that steady-state CaMKII activity in the spines depends on continuous Ca^{2+} influx via STIM2-regulated nSOC pathway (Figure 8A). Indeed, pharmacological blockade of nSOC or genetic deletion of STIM2 resulted in reduction of CaMKII activity in hippocampal neurons (Figure 7A). STIM2 protein abundantly expressed in hippocampal neurons (Figures 3 and S3), highly enriched in the mushroom spines (Figures 3D, 3E, and 3F), where it colocalizes with pCaMKII (Figure S6A). The role of STIM2 protein as mediator of nSOC pathway has been studied in the previous reports (Berna-Erro

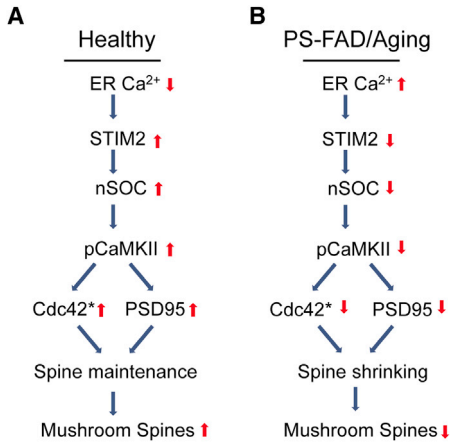

Figure 8. Role of STIM2-nSOC-CaMKII Pathway in Maintenance of Mushroom Postsynaptic Spines

(A) In healthy neurons, continuous Ca^{2+} influx via STIM2-nSOC pathway supports constant levels of CaMKII activity in the spines, leading to activation of Cdc42, stabilization of PSD95, and long-term stability of mushroom spines. (B) In PS-FAD and aging neurons, an increase in ER Ca^{2+} levels causes compensatory downregulation of STIM2 expression, impaired nSOC Ca^{2+} influx, reduced steady-state CaMKII activity in the spines, reduced Rac1/Cdc42 activity, destabilization of PSD95, and eventual loss of mushroom spines. Loss of mushroom spines results in memory impairment in aging and AD neurons. The symbol * indicates activated Rac1/cdc42 kinase.

et al., 2009; Gruszczynska-Biegala et al., 2011; Skibinska-Kijek et al., 2009), but the biological importance of SOC pathway in the nervous system has not been previously established. Our study points to unique and specific function of STIM2 as a regulator of synaptic nSOC pathway that is necessary for mushroom spine maintenance. Consistent with our hypothesis, conditional genetic deletion of *Stim2* resulted in dramatic reduction in synaptic nSOC and loss of mushroom spines in *Stim2* cKO neurons (Figure 5) and eventual death of hippocampal neurons (Figure S5). Interestingly, STIM1 could not compensate for loss of STIM2 in these experiments, most likely because of differences in Ca^{2+} sensitivity (Collins and Meyer, 2011) and subcellular localization (Figure 3) between these two proteins. Based on obtained results we concluded that STIM2-nSOC-CaMKII pathway plays an essential role in maintenance of mushroom spines in healthy neurons (Figure 8A).

STIM2-nSOC-CaMKII Pathway Is Compromised in Aging and AD Neurons

Our results further suggest that STIM2-nSOC-CaMKII pathway is compromised in aging and AD neurons, which leads to destabilization and loss of mushroom spines (Figure 8B). In our studies, we discovered that the levels of STIM2 protein, but not of STIM1 protein, were reduced in neuronal cultures or in hippocampus of PS1-M146V KI mice (Figures 3A, 3B, 4A, 4B, S4A, and S4B), in hippocampus of APPPS1 mice (Figures S4C and S4D), in hippocampus of aging mice (Figures 4C and 4D), and in cortical samples from sporadic AD human patients (Figures 4E, 4F, and S4E). Specific downregulation of STIM2 was previously reported for PS1-FAD patient fibroblasts (Bojarski et al., 2009), in agreement with our findings. Interestingly, we observed a quantitative correlation between cortical STIM2 expression levels and MMSE scores in human AD patients (Figure 4G). Consistent with reduced levels of STIM2 protein, we observed impaired nSOC in spines of PS1-M146V KI neurons (Figures 2D, 2E, and 2F) and reduced levels of CaMKII activity in PS1-M146V KI and aging neurons (Figures 7A, 7B, and 7C). Reduced levels of synaptic CaMKII activity has been previously reported for MCI and AD patients (Reese et al., 2011), in agreement with our model (Figure 8B). Heterologous expression of STIM2 protein was able to rescue synaptic nSOC (Figures 6A and 6B), CaMKII activity (Figures 7D, 7E, 7F, and 7G), and Rac1/Cdc42 activity (Figure S6B) in PS1-M146V KI neurons in culture and in vivo. In agreement with specific role of STIM2 protein, STIM1 was much less effective than STIM2 in ability to rescue nSOC and CaMKII activity in KI neurons in these experiments (Figures 6A, 6B, 7D, 7E, and S6). We propose that reduced fraction of mushroom spines in PS1-M146V KI neurons (Figure 1) is caused by reduced activity of STIM2-nSOC-CaMKII pathway (Figure 8B). Indeed, expression of STIM2, but not expression of STIM1, was able to rescue mushroom spine defects and PSD95 levels in PS1-M146V KI hippocampal neurons in culture and in vivo (Figures 6C, 6D, and 6F–6J). From these results we concluded that pharmacological upregulation of STIM2-nSOC-CaMKII pathway may provide a therapeutic benefit in age-related memory decline and in AD.

We would like to propose that reduction in STIM2 expression levels is a compensatory response to elevated ER Ca^{2+} levels in the postsynaptic spines. ER Ca^{2+} levels are increased in aging neurons (Foster, 2007; Gant et al., 2006; Kumar et al., 2009; Toescu and Verkhratsky, 2007). Many FAD mutations in presenilins, including PS1-M146V mutation and four other PS1-FAD mutations (L166P, A246E, E273A, and A426P) analyzed in our study (Figures S1C and S2B), disrupt ER Ca^{2+} leak function of presenilins and result in elevated ER Ca^{2+} levels (Leissring et al., 2000; Nelson et al., 2010; Nelson et al., 2007; Tu et al., 2006; Zhang et al., 2010). Thus, another potential therapeutic strategy is to develop a way to reduce synaptic ER Ca^{2+} levels in aging and AD neurons, which should result in upregulation of STIM2 expression and nSOC pathway. For example, mild inhibitors of ER SERCA Ca^{2+} pump may have a potential beneficial effect by reducing ER Ca^{2+} load in aging and AD neurons.

In conclusion, we discovered an essential role for STIM2 protein and synaptic nSOC pathway in long-term maintenance of mushroom spines (Figure 8A). We conclude that continuous Ca^{2+} influx via nSOC pathway leads to persistent activation of CaMKII at the spines and demonstrated that continuous activity of CaMKII is necessary for stability of the mushroom spines. We further demonstrated that STIM2-nSOC-CaMKII pathway is compromised in hippocampal neurons from PS1-M146V KI mice and from APPPS1 mice, in aging neurons, and in sporadic AD cortical samples due to reduced levels of STIM2 expression. We propose that disruption of STIM2-nSOC-CaMKII pathway contributes to synaptic loss and cognitive decline in aging and AD (Figure 8B). Our results suggest that upregulation of STIM2 expression levels or activity of synaptic nSOC pathway may yield therapeutic benefits for treatment of AD and other age-related memory disorders.

EXPERIMENTAL PROCEDURES

Please see the Supplemental Experimental Procedures for detailed methods on expression plasmids and viruses, Fura-2 Ca^{2+} imaging experiments, GCamP5.3 Ca^{2+} imaging experiments in hippocampal slices, dendritic spine analysis in mice hippocampus, immunohistochemistry, autopsy data, and clinico-pathological background of human patients, GTPases pull-down assays, and western blot analysis.

Animals

The PS1-M146V KI mice (Guo et al., 1999) were kindly provided by Hui Zheng (Baylor University). APPPS1 mice ($APP_{KM670/671NL}$, $PS1_{L166P}$) (Radde et al., 2006) were kindly provided by Mathias Jucker (Tubingen University). WT mice of the same strain (C57BL/6) were used in control experiments. *Stim2*$^{fl/fl}$ mice were generated as previously described (Oh-Hora et al., 2008). The mouse colonies were established and housed in a vivarium (four per cage) with 12 hr light/dark cycle at UT Southwestern Medical Center barrier facility. All procedures involving mice were approved by the Institutional Animal Care and Use Committee of the University of Texas Southwestern Medical Center at Dallas, in accord with the National Institutes of Health Guidelines for the Care and Use of Experimental Animals.

Dendritic Spine Analysis in Primary Hippocampal Neural Cultures

The hippocampal cultures of PS1-M146V KI, *Stim2*$^{fl/fl}$ and WT mice were established from postnatal day 0–1 pups and maintained in culture as we described previously (Zhang et al., 2010). For assessment of synapse morphology, hippocampal cultures were transfected with TD-Tomato plasmid at DIV7 using the calcium phosphate method and fixed (4% formaldehyde and 4% sucrose in PBS [pH 7.4]) at DIV14. A z stack of optical section was captured using 100× objective with a confocal microscope (Carl Zeiss Axiovert 100M with LSM510). At least 15 cultured neurons from three batches of cultures were used for quantitative analysis per genotype. Quantitative analysis for dendritic spines was performed by using NeuronStudio software package (Rodriguez et al., 2008). To classify the shape of neuronal spines in culture, we adapted an algorithm from published method (Rodriguez et al., 2008). In classification of spine shapes, we used the following cutoff values: aspect ratio for thin spines ($AR\_thin_{(crit)}$) = 2.5, head to neck ratio ($HNR_{(crit)}$) = 1.3, and head diameter (HD(crit)) = 0.45 μm. These values were defined and calculated exactly as described by Rodriguez et al. (2008).

GCamp5.3 Ca^{2+} Imaging Experiments

GCamp5.3 imaging experiments were performed as previously reported (Tian et al., 2009). Briefly, cultured WT and KI hippocampal neurons were transfected with GCamp5.3 expression plasmid using calcium phosphate transfection method at DIV7. The GCamp5.3 fluorescent images were collected using Olympus IX70 inverted epifluorescence microscope equipped with a 60× lens, Cascade 650 digital camera (Roper Scientific), and Prior Lumen 200 illuminator. The experiments were controlled by the MetaFluor image acquisition software package (Universal Imaging). To measure synaptic nSOC, the neurons were moved from artificial CSF (aCSF) to calcium-free media with 0.4 mM EGTA and 1 μM TG (thapsigargin) for 30 min and then returned to aCSF with addition of Ca^{2+} channels inhibitor cocktail (1 μM TTX, 10 μM AP5, 10 μM CNQX, and 50 μM nifedipine). The response to Ca^{2+} readdition was acquired using 488 nM excitation (GFP). Analysis of the data was performed using NIH Image J software. The region of interest (ROI) used in the image analysis was chosen to correspond to spines. All Ca^{2+} imaging experiments were done in room temperature.

Statistical Analyses

The results are presented as mean ±SEM. Statistical comparisons of results obtained in experiments were performed by Student's t test for two-group comparisons and one-way or two-way ANOVA followed by Tukey's test for multiple comparisons among more than two groups. The p values are indicated in the text and figure legends, as appropriate. The statistical analysis was performed by using n equals the number of independent neurons or spines analyzed or n equals the number of neuronal cultures and mice analyzed. In the second version of analysis, the mean of at least five neurons for each mouse or batch or culture was used as a single data point. Both methods of analysis yielded mostly similar results, although levels of statistical significance were lower when the second method was used. First method of analysis was used to generate figures for the paper. The detailed comparison of statistical results obtained by both methods is included to the paper as Table S2.

SUPPLEMENTAL INFORMATION

Supplemental Information includes six figures, two tables, one movie, and Supplemental Experimental Procedures and can be found with this article online at http://dx.doi.org/10.1016/j.neuron.2014.02.019.

ACKNOWLEDGMENTS

We are grateful to Hui Zheng for providing PS1-M146V KI mice, to Mathias Jucker for APPPS1 mice, to Lin Tian for providing Gcamp5.3 plasmid, to Thomas Südhof for providing Lenti-Cre constructs, to Xia Liang for technical assistance, to Leah Taylor for administrative assistance, and to Robin Hiesinger, Jen Liou, and Ege Kavalali for comments on the manuscript. We thank Dr. Beverly Davidson, Maria L. Scheel, and the staff of the University of Iowa Gene Transfer Vector Core for help with AAV production. We are grateful to Dr. Roger Rosenberg, Mr. Chan Foong, and Ms. Ellen Suen for help with collection and analysis of human clinical samples. I.B. is a holder of the Carl J. and Hortense M. Thomsen Chair in Alzheimer's Disease Research. This work was supported by McKnight Brain Disorders Award (I.B.); by Welch Foundation grant I-1754 (I.B.); by NIH grants R01NS080152 (I.B.), R01AI097302 (S.F.), and P30 AG12300 (C.W.); by the contract with the Russian Ministry of Science 11.G34.31.0056 (I.B.); and by the Shanghai Committee of Science and Technology (11DZ2260200) (N.J.X.), China 973 Program (2014CB965002) (N.J.X.), Pujiang Program (13PJ1405500) (N.J.X.), and National Natural Science Foundation of China grants 91232704 and 31271160 (N.J.X.).

Accepted: February 2, 2014
Published: April 2, 2014

REFERENCES

Akbari, Y., Hitt, B.D., Murphy, M.P., Dagher, N.N., Tseng, B.P., Green, K.N., Golde, T.E., and LaFerla, F.M. (2004). Presenilin regulates capacitative calcium entry dependently and independently of gamma-secretase activity. Biochem. Biophys. Res. Commun. *322*, 1145–1152.

Auffret, A., Gautheron, V., Mattson, M.P., Mariani, J., and Rovira, C. (2010). Progressive age-related impairment of the late long-term potentiation in Alzheimer's disease presenilin-1 mutant knock-in mice. J. Alzheimers Dis. *19*, 1021–1033.

Bandara, S., Malmersjö, S., and Meyer, T. (2013). Regulators of calcium homeostasis identified by inference of kinetic model parameters from live single cells perturbed by siRNA. Sci. Signal. *6*, ra56.

Berna-Erro, A., Braun, A., Kraft, R., Kleinschnitz, C., Schuhmann, M.K., Stegner, D., Wultsch, T., Eilers, J., Meuth, S.G., Stoll, G., and Nieswandt, B. (2009). STIM2 regulates capacitive Ca2+ entry in neurons and plays a key role in hypoxic neuronal cell death. Sci. Signal. *2*, ra67.

Bezprozvanny, I., and Hiesinger, P.R. (2013). The synaptic maintenance problem: membrane recycling, Ca2+ homeostasis and late onset degeneration. Mol. Neurodegener. *8*, 23.

Bezprozvanny, I., and Mattson, M.P. (2008). Neuronal calcium mishandling and the pathogenesis of Alzheimer's disease. Trends Neurosci. *31*, 454–463.

Bojarski, L., Pomorski, P., Szybinska, A., Drab, M., Skibinska-Kijek, A., Gruszczynska-Biegala, J., and Kuznicki, J. (2009). Presenilin-dependent expression of STIM proteins and dysregulation of capacitative Ca2+ entry in familial Alzheimer's disease. Biochim. Biophys. Acta *1793*, 1050–1057.

Bourne, J., and Harris, K.M. (2007). Do thin spines learn to be mushroom spines that remember? Curr. Opin. Neurobiol. *17*, 381–386.

Bourne, J.N., and Harris, K.M. (2008). Balancing structure and function at hippocampal dendritic spines. Annu. Rev. Neurosci. *31*, 47–67.

Chakroborty, S., Goussakov, I., Miller, M.B., and Stutzmann, G.E. (2009). Deviant ryanodine receptor-mediated calcium release resets synaptic homeostasis in presymptomatic 3xTg-AD mice. J. Neurosci. *29*, 9458–9470.

Collins, S.R., and Meyer, T. (2011). Evolutionary origins of STIM1 and STIM2 within ancient Ca2+ signaling systems. Trends Cell Biol. *21*, 202–211.

Das, H.K., Tchedre, K., and Mueller, B. (2012). Repression of transcription of presenilin-1 inhibits γ-secretase independent ER Ca^{2+} leak that is impaired by FAD mutations. J. Neurochem. *122*, 487–500.

DeKosky, S.T., and Scheff, S.W. (1990). Synapse loss in frontal cortex biopsies in Alzheimer's disease: correlation with cognitive severity. Ann. Neurol. *27*, 457–464.

Dickstein, D.L., Weaver, C.M., Luebke, J.I., and Hof, P.R. (2013). Dendritic spine changes associated with normal aging. Neuroscience *251*, 21–32.

Dumitriu, D., Rodriguez, A., and Morrison, J.H. (2011). High-throughput, detailed, cell-specific neuroanatomy of dendritic spines using microinjection and confocal microscopy. Nat. Protoc. *6*, 1391–1411.

Feng, B., Raghavachari, S., and Lisman, J. (2011). Quantitative estimates of the cytoplasmic, PSD, and NMDAR-bound pools of CaMKII in dendritic spines. Brain Res. *1419*, 46–52.

Foster, T.C. (2007). Calcium homeostasis and modulation of synaptic plasticity in the aged brain. Aging Cell *6*, 319–325.

Gant, J.C., Sama, M.M., Landfield, P.W., and Thibault, O. (2006). Early and simultaneous emergence of multiple hippocampal biomarkers of aging is mediated by Ca2+-induced Ca2+ release. J. Neurosci. *26*, 3482–3490.

Goussakov, I., Miller, M.B., and Stutzmann, G.E. (2010). NMDA-mediated Ca(2+) influx drives aberrant ryanodine receptor activation in dendrites of young Alzheimer's disease mice. J. Neurosci. *30*, 12128–12137.

Gruszczynska-Biegala, J., Pomorski, P., Wisniewska, M.B., and Kuznicki, J. (2011). Differential roles for STIM1 and STIM2 in store-operated calcium entry in rat neurons. PLoS ONE *6*, e19285.

Guo, Q., Fu, W., Sopher, B.L., Miller, M.W., Ware, C.B., Martin, G.M., and Mattson, M.P. (1999). Increased vulnerability of hippocampal neurons to excitotoxic necrosis in presenilin-1 mutant knock-in mice. Nat. Med. *5*, 101–106.

Herms, J., Schneider, I., Dewachter, I., Caluwaerts, N., Kretzschmar, H., and Van Leuven, F. (2003). Capacitive calcium entry is directly attenuated by mutant presenilin-1, independent of the expression of the amyloid precursor protein. J. Biol. Chem. *278*, 2484–2489.

Higley, M.J., and Sabatini, B.L. (2012). Calcium signaling in dendritic spines. Cold Spring Harb. Perspect. Biol. *4*, a005686.

Jack, C.R., Jr., Wiste, H.J., Weigand, S.D., Knopman, D.S., Lowe, V., Vemuri, P., Mielke, M.M., Jones, D.T., Senjem, M.L., Gunter, J.L., et al. (2013). Amyloid-first and neurodegeneration-first profiles characterize incident amyloid PET positivity. Neurology *81*, 1732–1740.

Kasai, H., Matsuzaki, M., Noguchi, J., Yasumatsu, N., and Nakahara, H. (2003). Structure-stability-function relationships of dendritic spines. Trends Neurosci. *26*, 360–368.

Knaus, U.G., Bamberg, A., and Bokoch, G.M. (2007). Rac and Rap GTPase activation assays. Methods Mol. Biol. *412*, 59–67.

Knobloch, M., and Mansuy, I.M. (2008). Dendritic spine loss and synaptic alterations in Alzheimer's disease. Mol. Neurobiol. *37*, 73–82.

Koffie, R.M., Hyman, B.T., and Spires-Jones, T.L. (2011). Alzheimer's disease: synapses gone cold. Mol. Neurodegener. *6*, 63.

Kumar, A., Bodhinathan, K., and Foster, T.C. (2009). Susceptibility to calcium dysregulation during brain aging. Front. Aging Neurosci *1*, http://dx.doi.org/10.3389/neuro.24.002.2009.

Leissring, M.A., Akbari, Y., Fanger, C.M., Cahalan, M.D., Mattson, M.P., and LaFerla, F.M. (2000). Capacitative calcium entry deficits and elevated luminal calcium content in mutant presenilin-1 knockin mice. J. Cell Biol. *149*, 793–798.

Li, X., Dang, S., Yan, C., Gong, X., Wang, J., and Shi, Y. (2013). Structure of a presenilin family intramembrane aspartate protease. Nature *493*, 56–61.

Lisman, J., Yasuda, R., and Raghavachari, S. (2012). Mechanisms of CaMKII action in long-term potentiation. Nat. Rev. Neurosci. *13*, 169–182.

Luebke, J.I., Weaver, C.M., Rocher, A.B., Rodriguez, A., Crimins, J.L., Dickstein, D.L., Wearne, S.L., and Hof, P.R. (2010). Dendritic vulnerability in neurodegenerative disease: insights from analyses of cortical pyramidal neurons in transgenic mouse models. Brain Struct. Funct. *214*, 181–199.

Murakoshi, H., and Yasuda, R. (2012). Postsynaptic signaling during plasticity of dendritic spines. Trends Neurosci. *35*, 135–143.

Nelson, O., Tu, H., Lei, T., Bentahir, M., de Strooper, B., and Bezprozvanny, I. (2007). Familial Alzheimer disease-linked mutations specifically disrupt Ca2+ leak function of presenilin 1. J. Clin. Invest. *117*, 1230–1239.

Nelson, O., Supnet, C., Liu, H., and Bezprozvanny, I. (2010). Familial Alzheimer's disease mutations in presenilins: effects on endoplasmic reticulum calcium homeostasis and correlation with clinical phenotypes. J. Alzheimers Dis. *21*, 781–793.

Oh-Hora, M., Yamashita, M., Hogan, P.G., Sharma, S., Lamperti, E., Chung, W., Prakriya, M., Feske, S., and Rao, A. (2008). Dual functions for the endoplasmic reticulum calcium sensors STIM1 and STIM2 in T cell activation and tolerance. Nat. Immunol. *9*, 432–443.

Penzes, P., Cahill, M.E., Jones, K.A., VanLeeuwen, J.E., and Woolfrey, K.M. (2011). Dendritic spine pathology in neuropsychiatric disorders. Nat. Neurosci. *14*, 285–293.

Popugaeva, E., and Bezprozvanny, I. (2013). Role of endoplasmic reticulum Ca2+ signaling in the pathogenesis of Alzheimer disease. Front. Mol. Neurosci *6*, http://dx.doi.org/10.3389/fnmol.2013.00029.

Popugaeva, E., Supnet, C., and Bezprozvanny, I. (2012). Presenilins, deranged calcium homeostasis, synaptic loss and dysfunction in Alzheimer's disease. Messenger *1*, 53–62.

Radde, R., Bolmont, T., Kaeser, S.A., Coomaraswamy, J., Lindau, D., Stoltze, L., Calhoun, M.E., Jäggi, F., Wolburg, H., Gengler, S., et al. (2006). Abeta42-driven cerebral amyloidosis in transgenic mice reveals early and robust pathology. EMBO Rep. *7*, 940–946.

Reese, L.C., Laezza, F., Woltjer, R., and Taglialatela, G. (2011). Dysregulated phosphorylation of Ca(2+) /calmodulin-dependent protein kinase II-α in the hippocampus of subjects with mild cognitive impairment and Alzheimer's disease. J. Neurochem. *119*, 791–804.

Riccio, A., Medhurst, A.D., Mattei, C., Kelsell, R.E., Calver, A.R., Randall, A.D., Benham, C.D., and Pangalos, M.N. (2002). mRNA distribution analysis of human TRPC family in CNS and peripheral tissues. Brain Res. Mol. Brain Res. *109*, 95–104.

Rodriguez, A., Ehlenberger, D.B., Dickstein, D.L., Hof, P.R., and Wearne, S.L. (2008). Automated three-dimensional detection and shape classification of dendritic spines from fluorescence microscopy images. PloS ONE. *3*, e1997.

Sanhueza, M., Fernandez-Villalobos, G., Stein, I.S., Kasumova, G., Zhang, P., Bayer, K.U., Otmakhov, N., Hell, J.W., and Lisman, J. (2011). Role of the CaMKII/NMDA receptor complex in the maintenance of synaptic strength. J. Neurosci. *31*, 9170–9178.

Selkoe, D.J. (2002). Alzheimer's disease is a synaptic failure. Science *298*, 789–791.

Skibinska-Kijek, A., Wisniewska, M.B., Gruszczynska-Biegala, J., Methner, A., and Kuznicki, J. (2009). Immunolocalization of STIM1 in the mouse brain. Acta Neurobiol. Exp. (Warsz.) *69*, 413–428.

Stutzmann, G.E., Caccamo, A., LaFerla, F.M., and Parker, I. (2004). Dysregulated IP3 signaling in cortical neurons of knock-in mice expressing an Alzheimer's-linked mutation in presenilin1 results in exaggerated Ca2+ signals and altered membrane excitability. J. Neurosci. *24*, 508–513.

Stutzmann, G.E., Smith, I., Caccamo, A., Oddo, S., Parker, I., and Laferla, F. (2007). Enhanced ryanodine-mediated calcium release in mutant PS1-expressing Alzheimer's mouse models. Ann. N Y Acad. Sci. *1097*, 265–277.

Sun, X., Beglopoulos, V., Mattson, M.P., and Shen, J. (2005). Hippocampal spatial memory impairments caused by the familial Alzheimer's disease-linked presenilin 1 M146V mutation. Neurodegener. Dis. *2*, 6–15.

Tackenberg, C., and Brandt, R. (2009). Divergent pathways mediate spine alterations and cell death induced by amyloid-beta, wild-type tau, and R406W tau. J. Neurosci. *29*, 14439–14450.

Tackenberg, C., Ghori, A., and Brandt, R. (2009). Thin, stubby or mushroom: spine pathology in Alzheimer's disease. Curr. Alzheimer Res. *6*, 261–268.

Tian, L., Hires, S.A., Mao, T., Huber, D., Chiappe, M.E., Chalasani, S.H., Petreanu, L., Akerboom, J., McKinney, S.A., Schreiter, E.R., et al. (2009). Imaging neural activity in worms, flies and mice with improved GCaMP calcium indicators. Nat. Methods *6*, 875–881.

Toescu, E.C., and Verkhratsky, A. (2007). The importance of being subtle: small changes in calcium homeostasis control cognitive decline in normal aging. Aging Cell *6*, 267–273.

Tu, H., Nelson, O., Bezprozvanny, A., Wang, Z., Lee, S.F., Hao, Y.H., Serneels, L., De Strooper, B., Yu, G., and Bezprozvanny, I. (2006). Presenilins form ER Ca2+ leak channels, a function disrupted by familial Alzheimer's disease-linked mutations. Cell *126*, 981–993.

Wang, R., Dineley, K.T., Sweatt, J.D., and Zheng, H. (2004). Presenilin 1 familial Alzheimer's disease mutation leads to defective associative learning and impaired adult neurogenesis. Neuroscience *126*, 305–312.

Wilcox, K.C., Lacor, P.N., Pitt, J., and Klein, W.L. (2011). Aβ oligomer-induced synapse degeneration in Alzheimer's disease. Cell. Mol. Neurobiol. *31*, 939–948.

Wirth, M., Madison, C.M., Rabinovici, G.D., Oh, H., Landau, S.M., and Jagust, W.J. (2013a). Alzheimer's disease neurodegenerative biomarkers are associated with decreased cognitive function but not β-amyloid in cognitively normal older individuals. J. Neurosci. *33*, 5553–5563.

Wirth, M., Villeneuve, S., Haase, C.M., Madison, C.M., Oh, H., Landau, S.M., Rabinovici, G.D., and Jagust, W.J. (2013b). Associations between Alzheimer disease biomarkers, neurodegeneration, and cognition in cognitively normal older people. JAMA Neurol *70*, 1512–1519.

Wu, J., Shih, H.P., Vigont, V., Hrdlicka, L., Diggins, L., Singh, C., Mahoney, M., Chesworth, R., Shapiro, G., Zimina, O., et al. (2011). Neuronal store-operated calcium entry pathway as a novel therapeutic target for Huntington's disease treatment. Chem. Biol. *18*, 777–793.

Yasuda, R., Sabatini, B.L., and Svoboda, K. (2003). Plasticity of calcium channels in dendritic spines. Nat. Neurosci. *6*, 948–955.

Yoo, A.S., Cheng, I., Chung, S., Grenfell, T.Z., Lee, H., Pack-Chung, E., Handler, M., Shen, J., Xia, W., Tesco, G., et al. (2000). Presenilin-mediated modulation of capacitative calcium entry. Neuron *27*, 561–572.

Zhang, H., Sun, S., Herreman, A., De Strooper, B., and Bezprozvanny, I. (2010). Role of presenilins in neuronal calcium homeostasis. J. Neurosci. *30*, 8566–8580.

Zhou, J., Du, W., Zhou, K., Tai, Y., Yao, H., Jia, Y., Ding, Y., and Wang, Y. (2008). Critical role of TRPC6 channels in the formation of excitatory synapses. Nat. Neurosci. *11*, 741–743.